Spectroscopic Characterization of Solid−Solid Transitions in Model Compounds for Copolymers Containing Sequential Thioethylene Units

Jeno Muthiah, C. Gregory Johnson, Robert D. Thompson, and Lon J. Mathias*

Department of Polymer Science, University of Southern Mississippi, Hattiesburg, Mississippi 39406-0076

Received March 1, 1995; Revised Manuscript Received August 16, 1995[⊗]

ABSTRACT: In this paper, we describe the thermal and spectroscopic analysis of oligo(thioethylene) model compounds for copolymers containing sequential thioethylene units. Many thioethylene copolymers and model compounds show multiple thermal transitions by DSC, although the molecular-level behavior associated with such transitions is not known. The model compounds studied here consist of $CH_3(CH_2)_9S(CH_2CH_2S)_n(CH_2)_9CH_3$, with $n = 1-5$. For $n = 1$, a crystal structure was identified by WAXD, ^{13}C CP/MAS, and FT-IR analysis that was different than the others. For all other model compounds (with $n = 2-5$), the crystal structures were similar with increased interactions between molecules as n increased, caused by increasing numbers of thioethylene segments resulting in more favorable gauche conformations at the internal C−S bonds. This leads to packing similar to that of poly(thioethylene) and causes the melting points of higher oligo(thioethylene) analogs to be higher than those of linear alkanes of similar lengths. From ^{13}C CP/MAS results, carbons adjacent to sulfur experience a shielding of ca. 0.6 ppm for every γ-gauche interaction in the solid state and a 0.8 ppm upfield shift for each β thioether in the trans conformation. In compounds with a mixture of trans and gauche conformers at the C−S bonds, librational motion increased the trans isomer content at temperatures above ambient but below melting transitions observed by DSC. This conformational motion was identified by ^{13}C CP/MAS, ^{13}C HP/MAS, Raman, and IR analysis. For two of the models, a distinct solid−solid transition (below the melting point) occurred to accommodate changes in thioethylene segment conformations. At this transition, an all-trans conformation was observed with increased intermolecular spacing similar to what is seen by WAXD for the lowest oligo(thioethylene) analog ($n = 1$) at room temperature. This thermal lattice expansion was observed for the model compound with five thioether moieties as discontinuous changes in solid-state ^{13}C NMR chemical shifts and C−D bond splitting and changes in the intensities and frequencies of IR vibrational modes. These crystal and conformational changes were completely reversible as monitored by ^{13}C and ^{2}H NMR, IR, Raman, and DSC.

Introduction

We have been studying copolymers of thioethylene and oxyethylene possessing sequential repeat units to synthetically evaluate the combined or averaged properties derived from the number and distribution of each moiety along the chain. We have reported the synthesis of sequential copolymers[1] which showed unusual thermal behavior by DSC with two endotherms on either side of an exotherm.[2] When observed on a microscope hot stage, the samples did not undergo any visual transformation at the first endothermic transition, indicating that macroscopic order was maintained above this temperature and up to the melt. Multiple transitions were also observed in two different families of copolymers made by interfacial condensation of ethanedithiol and various dibromoalkanes[3,4] and by polymerization of ethanedithiol with acetone and formaldehyde.[5] Such solid−solid transitions have been observed on heating many other polymer systems, including poly(butylene terephthalate),[6] poly(ethylene terephthalate),[7] various polyamides,[8−10] and polybutadiene.[11] Similar to these systems, all the thioether copolymers showed only one crystallization exotherm during the DSC cooling run.

Since multiple transitions are seen on heating many of these sulfur-containing polymers, understanding their molecular basis is desirable and may lead to improved processability of homo- and copolymers. In order to correlate the multiple transitions in copolymers to molecular-level behavior, we have synthesized model compounds of structure $CH_3(CH_2)_9S(CH_2CH_2S)_n(CH_2)_9CH_3$ containing multiple thioethylene units (n varying from 1 to 5). Ambient temperature characterization involved ^{13}C CP/MAS (cross-polarized/magic angle spinning) and HP/MAS (high-power decoupled/magic angle spinning) NMR, IR, and Raman to examine the effect of increasing thioethylene units on conformation and motion. Variable-temperature solid-state ^{13}C and ^{2}H NMR, Raman, and IR analysis were employed in analyzing the changes in chemical environment, rigidity, and vibrational modes with respect to transition temperatures observed by DSC. X-ray powder diffraction provided insight into the influence of the thioethylene segment length on intermolecular distances and packing.

Experimental Section

1,2-Dimercaptoethane (**1**), decyl mercaptan, dichloroethane, 1-bromodecane, sodium borohydride, sodium borodeuteride, thiourea, 3,6-dithiaoctane-1,8-diol, thiodiglycolic acid, and boron trifluoride etherate were purchased from Aldrich Chemical Co. 2-Mercaptoethyl thioether (**2**) was obtained from Nisso Maruzen Chemical Co. and distilled before use. Tetrahydrofuran (THF) was dried over CaH and distilled before use. Other solvents were used without further purification.

Thermal analysis was carried out with a Perkin-Elmer DSC 7 equipped with an IBM microcomputer. Solution ^{1}H and ^{13}C NMR spectra were obtained on Bruker AC-200 and AC-300 spectrometers. X-ray data were obtained on a Siemens XDP-700P using Cu Kα radiation. ^{13}C CP/MAS and HP/MAS data

[⊗] Abstract published in *Advance ACS Abstracts,* October 15, 1995.

0024-9297/95/2228-7796$09.00/0

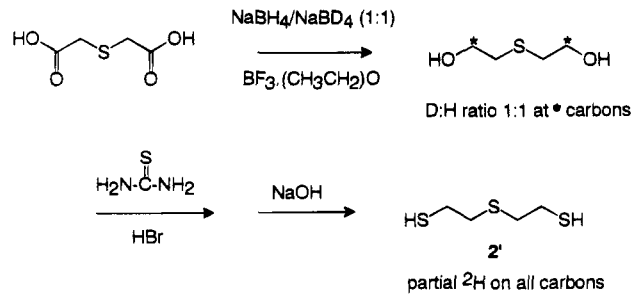

Figure 1. Synthesis of partially deuterated 2-mercaptoethyl thioether (**2′**).

were obtained on a Bruker MSL-400 equipped with a standard Bruker 4 mm MAS probe operating at 100.6 MHz. The ^1H 90° pulse was 4.6 μs, the ^1H 180° pulse was 9.2 μs, the contact time was 1 ms, the ringdown delay was 14 μs, and the acquisition time was 45 ms. The ^1H T_1 values were determined at ambient temperature, 84 °C, and 90 °C, and the recycle delays used for ^{13}C measurements at these temperatures and above were at least 5 times the ^1H T_1 in seconds. The data points were 4K zero-filled to 8K before Fourier transformation. A line-broadening constant of 5 Hz was used as a multiplier.

^2H NMR spectra were obtained at 61.424 MHz using a Doty 8 mm probe in a Bruker NMR instrument (400 MHz proton frequency). All points to the left of the top of the fid were discarded and the Fourier transformation done after exponential multiplication with a line-broadening factor of 500 kHz in all cases. Spectra were acquired using the solid echo pulse sequence with a 90° pulse width of 3.7 μs and a recycle time of 1.5 s. Temperature was controlled using the Bruker Eurotherm digital temperature controller. Temperatures within the sample area are estimated to be accurate to within ±2 °C based on previous calibrations and correlation with melt determinations by thermal analysis. The sample was equilibrated for 20 min at each temperature before 1048 scans were collected.

IR analysis was performed on a Perkin-Elmer 1600 FT-IR operating at a resolution of 2 cm^{-1}. An Omega variable-temperature unit was used for acquisition of high-temperature IR spectra. Sample preparation involved melting the sample between two KBr IR windows and cooling back to room temperature. Samples were maintained at each temperature for 30 min before collection of spectra. Raman measurements were made on a Bruker IFS 88 spectrometer with an FRA 106 Raman module using a laser power of 500–600 mW to minimize sample heating. It should be pointed out that temperatures given for the various variable-temperature spectroscopic studies are nominal (uncorrected) values and do not always agree exactly with each other. This is due to differences in location of thermocouples, uncontrollable (but slight) temperature gradients or inhomogeneities, and differences in frequency of measurement (for NMR experiments). While quantitative agreement of temperatures is not exact, qualitative values and correlations with molecular transitions are excellent.

2-Mercaptoethyl Thioether-d_2 (2′). The synthesis of **2′** is given in Figure 1. Sodium borodeuteride and sodium borohydride (2.5 g of each, 125 mmol) in 200 mL of dried THF were stirred using a mechanical stirrer for 15 min under N_2 at 10–15 °C until an emulsion formed. Boron trifluoride etherate (25.3 g, 179 mmol) diluted with 100 mL of THF was then added over a period of 2 h while the temperature was maintained at 10–15 °C. During the addition of $(CH_3CH_2)_2O$–BF_3, a white precipitate formed. After another 30 min, thiodiglycolic acid (10 g, 66.6 mmol) in 200 mL of THF was added over a period of 3 h; gas evolution was observed. Stirring was continued for another 6 h, and the reaction was quenched by adding 100 mL of a THF:H_2O (50:50) mixture. To the clear solution, 25 g of K_2CO_3 was added, causing formation of two phases. Gas chromatography of the crude organic phase showed 91% thiodiethanol. Distillation yielded 5.5 g of thiodiethanol (yield 69%). The ^{13}C NMR proton-coupled spectrum confirmed incorporation of deuterium. Conversion of the thiodiethanol to 2-mercaptoethyl thioether was carried out using the procedure for **3** described below. This yielded 4.6 g (30 mmol) of **2′** after distillation (overall yield 45% from thiodiglycolic acid).

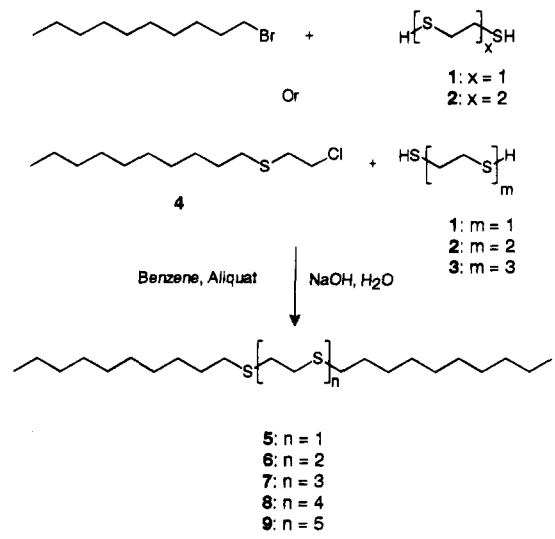

Figure 2. General syntheses of $CH_3(CH_2)_9S(CH_2CH_2S)_n(CH_2)_9CH_3$.

3,6-Dithiaoctane-1,8-dithiol (3). 3,6-Dithiaoctane-1,8-dithiol (**3**) was synthesized according to the following procedure.[12] To a round-bottom flask containing 3,6-dithiaoctane-1,8-diol (10.35 g, 56.8 mmol) and thiourea (8.7 g, 114 mmol) was added 19.5 mL of 48% HBr (170 mmol) under N_2. The temperature was raised to 110 °C and maintained there for 9 h with stirring. The reaction mixture was then cooled to room temperature and NaOH (6.84 g, 17 mmol) in 115 mL of water was added slowly, during which a white solid formed. The mixture was heated at reflux for 10 h, causing an immiscible organic layer to form. The mixture was cooled, neutralized with dilute HCl, and extracted with CH_2Cl_2. The organic phase was separated and solvent removed by rotary evaporation. Vacuum distillation at 155 °C (2.3 mmHg) yielded 96% pure **3**: 5.7 g, 47% yield; ^{13}C NMR ($CDCl_3$) δ 24.7 ($\mathbf{C}H_2SH$), 32.2 ($S\mathbf{C}H_2CH_2SH$), 36.3 ($\mathbf{C}H_2SCH_2CH_2SH$).

2-Chloroethyl *n*-Decyl Thioether (4). Sodium hydride (1.65 g, 68.7 mmol) was carefully added to a solution of decyl mercaptan (10 g, 57.4 mmol) in 100 mL of THF; gas was evolved. The solution was stirred for 6 h and transferred to an addition funnel. This solution was then added over 30 min to a flask containing 1,2-dichloroethane (115 g, 1.16 mol). The mixture was then heated at reflux overnight. The solvent was removed by rotary evaporation and the product was taken up in CH_2Cl_2. Rotary evaporation of the CH_2Cl_2 solution yielded 11.2 g of product that was 93.0% pure by GC. Distillation under vacuum yielded **1** (9.5 g, 40 mmol, 70% yield, 97% pure by GC).

General Procedure for $CH_3(CH_2)_9S(CH_2CH_2S)_n(CH_2)_9CH_3$ (5–9 and 8′). Model compounds of structure $CH_3(CH_2)_9S(CH_2CH_2S)_n(CH_2)_9CH_3$ with n varying from 1 to 5 (**5**–**9**) were synthesized under phase transfer conditions. The general synthetic scheme is given in Figure 2. A typical procedure involved mixing **2** (1.302 g, 8.4 mmol) and **4** (4.0 g, 16.9 mmol) in 20 mL of benzene at room temperature with Aliquat 336 (Aldrich) (0.17 g, 0.42 mmol). To this was added NaOH (1.0 g, 25 mmol) as a 1.25 M solution in deionized water. The solution was heated at reflux overnight, after which the organic phase was separated and extracted with water. Removal of the organic solvent followed by recrystallization from an appropriate solvent (THF for **5** and **6** and $CHCl_3$ for the others) yielded crystalline product. Synthesis of **8′** was achieved by reacting **2′** with **4** in a similar fashion. Recrystallization of **8** from $CHCl_3$ yielded white crystals: 3.2 g, 69% yield; ^{13}C NMR ($CDCl_3$) δ 14.0 ($\mathbf{C}H_3$), 22.6 ($\mathbf{C}H_2CH_3$), 28.8, 29.2 ($\mathbf{C}H_2)_5CH_2CH_2CH_3$), 29.5, 29.7 ($\mathbf{C}H_2S$), 31.8 ($\mathbf{C}H_2CH_2CH_3$, $SCH_2\mathbf{C}H_2C_8H_{17}$), 32.2 ($S\mathbf{C}H_2C_9H_{19}$), 32.4 ($S\mathbf{C}H_2CH_2S$).

Table 1. Yields, Melting Points, and Submelting Transitions (in Parentheses) of Model Compounds 5–9

	yield (%)	mp (°C)
5	80	43
6	87	57
7	81	77 (65)
8	69	97 (83)
9	61	110

Results and Discussion

The behavior of the model compounds was found to be complicated, requiring a variety of characterization methods, each of which focuses on a particular molecular segment or type of interaction, to fully understand the solid-state packing of all members of the series and the changes in packing which occur on heating. The sections following deal with (1) synthesis and initial DSC results for each series member in comparison with the others and with polyethylene (PE) and poly(thioethylene) (PTE); (2) the room temperature packing of members of the series, where changes in conformation occur because of the change in ratio of internal thioethylene segments to terminal alkane units; and (3) detailed variable-temperature analysis of a representative member of the series (**8**) to understand the changes in segmental packing and motion which occur on going through a first-order premelting transition seen for many of these compounds and their analogous homo- and copolymers. The ultimate goal of this paper is to use the knowledge of molecular packing and thermal changes for model compounds generated here to understand the behavior of various sequential copolymers containing thioethylene units.

Synthetic and DSC Results. Synthesis of **2′** gave good results using the procedure described here. An alternative procedure involving addition of the borohydride to a THF solution of thiodiglycolic acid (similar to a reported procedure)[13] resulted in gelation, and analysis of the product showed very low conversion of acids to alcohols. Incorporation of ^2H at the carbon β to sulfur in thiodiethanol was confirmed by comparing ^{13}C proton coupled and decoupled spectra. Conversion of thiodiethanol to **2′** led to scrambling of ^2H to both carbons α and β to the central sulfur atom through formation of a three-membered cyclic sulfonium intermediate that results in the interconversion of methylene units. A similar intermediate has been reported for related substitution reactions on terminal carbons β to a thioether moiety.[14] Compounds **3** and **4** were also synthesized for this study as they were not commercially available.

The yields and DSC melting points of **5–9** are given in Table 1; the melting point of partially deuterated **8′** was the same as that of **8**. Melting points of model compounds increased steadily with increase in the number of thioethylene units. For $n = 1$ and 2, the melting points (43 and 57 °C) were very close to those for the linear alkanes with equal numbers of backbone atoms ($C_{24}H_{50}$ and $C_{27}H_{56}$, mp 48 and 59 °C, respectively). For $n > 2$, however, the melting points of the model compounds increased more rapidly with chain length than those of the corresponding linear alkanes (Figure 3), indicating different packing and crystalline interactions for the longer thioethylene segments. It should be pointed out that the asymptotic melting points for the two infinite chains are ca. 212 °C for PTE and ca. 142 °C for PE.

The higher melting points for the thioether materials are in apparent intuitive contradiction with the fact that

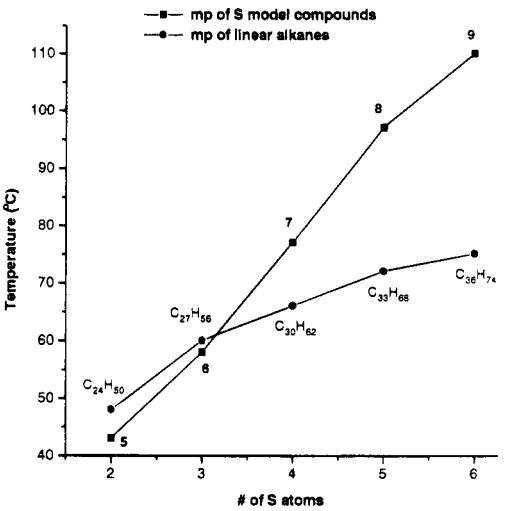

Figure 3. Melting point comparisons of **5–9** with linear alkanes possessing the same total number of atoms.

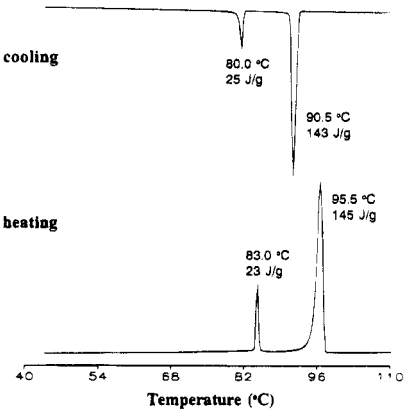

Figure 4. DSC heating and cooling thermograms of **8** (transition temperatures, heats in J/g).

the C–S–C segment has greater bond lengths and flexibility than a corresponding C–C–C unit. The thermodynamically stable conformations around C–C and C–S bonds are trans and gauche, respectively, with rotational energy barriers for each of about 3.0 and only 0.5 kcal/mol.[15,16] The all-trans conformation preferred for PE and the C–C–C–C moiety in general allows close packing and optimal summation of the weakest intermolecular forces, van der Waals interactions. For PTE, the more stable gauche isomer at the C–C–S–C bond forms a 2_1 glide plane in the solid polymer, which orients alternating sulfur atoms at 180° with respect to each other and introduces strong dipole interactions between C–S–C groups in adjacent chains. Summation of these dipolar interactions contributes to its high melting point compared to PE.[17]

Of further interest in the DSC thermograms of **7** and **8** are the two distinct endotherms and exotherms on heating and cooling, respectively. Both heating and cooling traces for **8** are given in Figure 4 (both are reproducible) along with the ΔH values (in J/g) of the two transitions seen in each. Temperatures corresponding to melting and submelting transitions are given in Table 1. The window between the two endotherms is reduced with increase in the length of the oligo(thioethylene) segment; a broad melting endotherm without a separate submelting transition for **9** may reflect merging of the two transitions.

Questions to be addressed in the next two sections include the following: (1) What changes in molecular

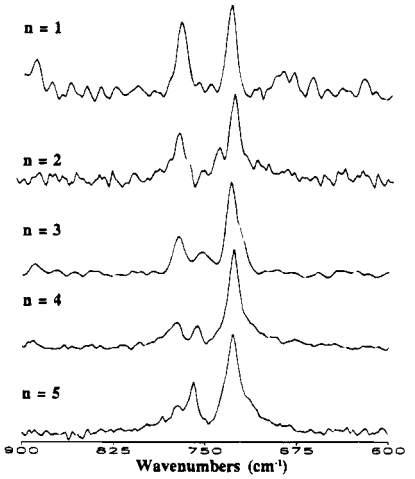

Figure 5. Raman spectra of $CH_3(CH_2)_9S(CH_2CH_2S)_n(CH_2)_9CH_3$ with n varying from 1 to 5 from top to bottom.

packing occur in the series that results in the behavior seen in Figure 3; i.e., how does the preferred conformation of the alkyl segment (all-trans) interact with that of the thioethylene segments? (2) What is the nature of the first-order premelt transition seen for **7** and **8**? Because this initial endotherm is more pronounced for **8**, this material was chosen for detailed investigation.

Room Temperature Analysis of $CH_3(CH_2)_9S(CH_2CH_2S)_n(CH_2)_9CH_3$ (5–8) Raman Results. The conformational preference at the C–S bond with increasing thioethylene units can be characterized by Raman analysis between 900 and 600 cm^{-1} corresponding to the C–S stretching region. Both asymmetric and symmetric stretches are observed, but only the asymmetric peaks contain conformational information. In ethyl methyl thioether, the trans and gauche conformers at the C–S bond show peaks at 725 and 655 cm^{-1}, respectively.[18] In 2,5-dithiohexane, the trans and gauche isomer peaks occur at 725 and 700 cm^{-1}, respectively.[19] In PTE, peaks are seen at 760 and 730 cm^{-1} for C–S asymmetric and symmetric stretches, respectively.[20] The former corresponds to thioethylene units frozen in the more stable gauche conformation, but at a value higher than the ca. 725 cm^{-1} gauche peaks seen for low molecular weight compounds in solution or in the melt.

Room temperature (solid state) Raman spectra in the C–S stretching region of the model compounds are given in Figure 5. The asymmetric C–S stretch at 760 cm^{-1} increases with number of sequential thioethylene units while a band at 775 cm^{-1} decreases. The latter peak is assigned to the trans conformers of thioethylene units (involving carbons "6" and "7" in **5**) adjacent to the long aliphatic chains locked in the all-trans conformation (carbons marked "5" in **5**). That is, for the lowest member of the series, the trans polymethylene chain induces a trans conformation at the C–S bonds as illustrated in Figure 6. Thus, the gauche band at 760 cm^{-1} is absent when $n = 1$ but increases in intensity with $n > 1$. For **6–9**, bands corresponding to both trans and gauche isomers are (and should be) present, with the peak at 760 cm^{-1} increasing in intensity as n increases; increases and decreases used here describe changes relative to the intense symmetric stretch at ca. 730 cm^{-1}. A key observation here is that the all-trans conformation of the terminal decyl group induces trans conformations at the adjacent thioether units in all of the model compounds, and the contribution of these units to the spectral data discussed in the next sections must be kept in mind.

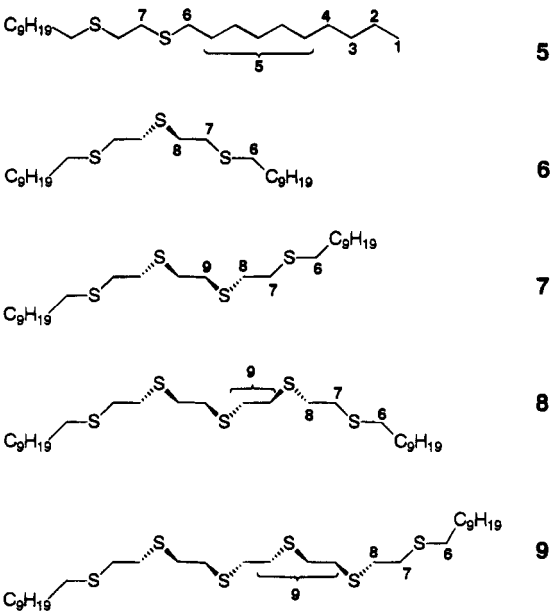

Figure 6. Preferred conformations at thioethylene segments in model compounds (straight lines in the plane and wedges out of plane) and carbon designations for peaks observed in ^{13}C CP/MAS spectra.

The increase in C–S gauche conformation in higher oligo(thioethylene) analogs is represented in Figure 6 for **5–9**; i.e., these structures represent a first guess at molecular packing conformations in the crystalline domains of each compound that are consistant with Raman results. Thus, in all the model compounds, there are four C–S bonds in trans conformations at the C–S groups closest to the alkyl segments while the number of gauche bonds for internal thioethylene segments increases linearly from 2 to 8 in going from **6** to **9** (involving carbons labeled 8 and 9 in Figure 6). The increase in gauche content is reflected in the gradual shift in peak position from 752 cm^{-1} for **6** to 759 cm^{-1} in **9**; the asymptotic value for PTE is 760 cm^{-1}.

The C–H stretching region shows similar results, with the C–H asymmetric stretch at 2954 cm^{-1} for the gauche isomer (similar to PTE) increasing as n increases. At the same time, a peak at 2935 cm^{-1} (which we believe is associated with the trans C–S conformation) decreases in intensity. Neither the C–H nor the C–S symmetric stretches (2921 and 730 cm^{-1}) are influenced by the number of sequential thioethylene units, supporting a previous claim that only the asymmetric C–S stretches are sensitive to conformation.[21] The model compounds have additional (compared to PTE) but uniform peaks at 2883 and 2849 cm^{-1} for their alkyl segments in all-trans conformations.[22]

Solid-State NMR Results. ^{13}C CP/MAS spectra of **5–9** are given in Figure 7, and the peak positions are compared in Table 2. The proposed conformations at the thioethylene and decyl segments given in Figure 6 include carbon labels from the methyl group to the central thioethylene units. Spectral interpretation was complicated by the fact that compounds **5** and **9** displayed anomalous behavior compared to that of **6–8**. Compound **5** was unique in possessing no thioethylene gauche conformations in the solid state, resulting in a type of crystal packing that caused 0.8–0.9 downfield shifts in peaks for those carbons attached to sulfur and 0.4–0.6 ppm downfield shifts for all alkyl carbons except methyl. Compound **9** displayed peaks for the sulfur carbons consistent with compounds **6–8**, but the alkyl

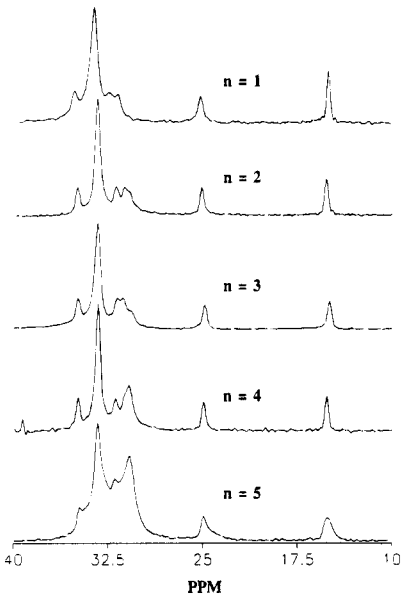

Figure 7. ^{13}C CP/MAS spectra of $CH_3(CH_2)_9S(CH_2CH_2S)_n(CH_2)_9CH_3$ with n varying from 1 to 5 from top to bottom.

Table 2. Chemical Shifts for Carbons (As Numbered in Figure 5) of Model Compounds 5–9 (Values in Parentheses Are for the Carbon 7 Peak Merged with that of Carbon 9 in 7, 8, and 9)

carbon	5	6	7	8	9
1	15.1	15.2	15.1	15.2	14.8
2	25.5	25.1	25.0	25.0	24.8
3	35.6	35.0	35.0	34.9	34.8
4	34.0	33.4	33.5	33.4	33.3
5	34.0	33.4	33.5	33.4	33.3
6	32.8	31.9	31.9	32.0	31.9
7	32.0	31.2	31.3	31.2[b]	(30.8)[d]
8		30.8	30.7[a]	30.8[c]	(30.8)[d]
9			30.7[a]	30.8[c]	30.8[d]

[a] Carbons 8 and 9 of compared **7** appear as a broad peak at 30.7 ppm. [b] Carbon 7 of compound **8** appears as a shoulder on the 30.8 ppm peak. [c] Carbons 8 and 9 of compound **8** appear as a broad peak at 30.8 ppm. [d] Carbons 7, 8, and 9 of compound **9** appear as a broad peak between 31.6 and 29.5 ppm.

carbon peaks were all shifted upfield by 0.1–0.4 ppm, especially the terminal carbons 1–3.

The central CH_2's of the decyl chain (4 and 5) appear at 34.0 ppm for **5** and 33.4 ppm in **6**–**9**. The fact that *all* CH_2's in **5** are significantly less shielded relative to the other model compounds suggests a totally different type of crystal packing for this material. The changes in chemical shift are similar to what has been seen in PE: in the orthorhombic crystal form, the CH_2's appear at 33.1 ppm, while in the monoclinic form they are at 34.0 ppm.[23] The other possibility of a rotator phase existing at ambient temperature in **5** is unlikely since the chain-end carbon peaks generally move upfield on forming the rotator phase and here they are shifted downfield.[24]

In the region between 30.0 and 33.0 ppm there are multiple peaks for all the model compounds corresponding to carbons adjacent to sulfurs. The multiple peaks indicate different amounts of shielding related to changing composition and conformational variations around the C–S bonds. Having data from a range of model compounds with systematic increase in thioethylene content allows elucidation of the contributions from through-bond and through-space effects. Three possible situations at the methylene units are shown in Figure 6 for the series of model compounds. For **5**, there are only two types of carbons next to sulfur atoms (carbons 6 and 7). Both have γ-carbon atoms on both sides in trans conformations, one on the decyl group side and one on the thioethylene segment side (Raman data show that there are no gauche isomers at the C–S bonds and there is therefore no gauche shielding contribution expected in the NMR data). Methylene unit 7 (between two sulfur atoms) experiences a similar conformational interaction to 6 from γ atoms (no gauche shielding) on both sides plus an additional *shielding* effect caused by the β sulfur through a trans conformation at the C–C–S–C moiety (vide infra); this is apparently a through-bond effect. Hence, carbon 7 appears upfield (at 32.0 ppm) compared to 6 at 32.8 ppm, and the trans β sulfur shielding effect is thus estimated to be approximately 0.8 ppm. A similar (but conformationally averaged) upfield shift of about 0.4 ppm was observed for the methylene carbon β to sulfur in liquid octyl methyl sulfide.

For solid **6**, the C–S bonds associated with the outermost sulfur atoms are still in trans conformations but with central C–S bonds in gauche conformations. The ratio of trans–trans (tt, 6) to trans–gauche (tg, 7 and 8) carbons is 1:2 but there are three equal-intensity peaks in Figure 7 for these three carbons. With respect to chemical environment, carbon 6 experiences trans–trans (tt) environments at the γ atoms (similar to 6 in **5**) and appears at 32.0 ppm, upfield compared to 6 in **5** (32.8 ppm) due to different crystal packing; this shift is similar to the upfield shift of about 0.6 ppm seen also for the central CH_2 units in the decyl segment of **6** compared to **5**. Carbon 7 of the internal C–S bonds, however, has a gauche conformation (g) along the inward direction but is still trans (t) with respect to the carbon next to 6 as shown in Figure 6. The carbon 7 peak seen at 32.0 ppm for **5** moves upfield by 0.6 ppm to 31.4 ppm due again to different crystal packing plus two opposing conformational effects. As compared to carbon 7 in **5**, the trans β sulfur shielding (−0.8 ppm) at this carbon is removed and one γ-gauche shielding (−0.9 ppm) is introduced. That is, carbon 7 does *not* experience a trans β sulfur shielding of approximately 0.8 ppm and thus should shift downfield to 32.2 ppm (31.4 + 0.8). The fact that it is actually seen at 31.3 ppm is attributed to the γ-gauche shielding (ca. −0.9 ppm) due to a gauche conformation at one of the adjacent C–S bonds. Carbon 8 has conformations similar to 7 (tg) at the adjacent C–S bonds. However, as seen in Figure 6, carbon 8 experiences *both* β sulfur and γ-gauche shieldings and is observed at 30.8 ppm, upfield relative to carbon 7. Thus, there are two conformationally dependent effects that determine the chemical shifts for methylene units adjacent to sulfur in these compounds, the γ-gauche and trans β-sulfur shielding, both of which cause 0.7–0.9 ppm upfield shifts. Another important observation is that the γ-gauche shielding involving C–S bonds is much smaller than the γ-gauche shielding in linear alkanes (ca. 3–5 ppm) due to the longer C–S bonds and wider C–S–C angles diminishing the through-space shielding because the interacting groups are farther apart.

Based on these empirically evaluated shielding effects, analysis can now be extended to higher oligo(thioethylene) models. Incorporation of one more thioethylene unit (in **7**) results in a total 1:1 ratio of trans to gauche isomers at C–S bonds. In addition to carbons 6, 7, and 8, a new set of carbons that have gauche interactions on *both* sides (gg) occurs at position 9.

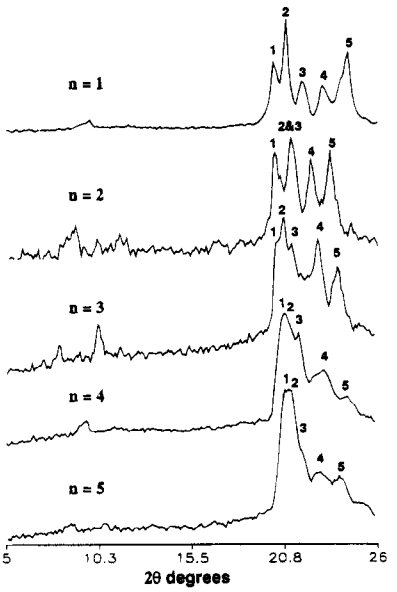

Figure 8. WAXD patterns of $CH_3(CH_2)_9S(CH_2CH_2S)_n(CH_2)_9CH_3$.

Carbons 6, 7, and 8 should appear at the same chemical shifts as in **6**. Carbon 9, on the other hand, does not experience trans β sulfur shielding but does have an additional γ-gauche interaction. Since these two effects are almost equal, 9 is observed at the same position as carbon 8 in **6**, at 30.7 ppm. This peak is also observed in PTE, which has all carbons in gg environments. The ratio of the 6, 7, and 8 + 9 carbons in **7** should thus correspond to 1:1:2 peak intensities as is actually seen in its ^{13}C CP/MAS spectrum (the peak at 30.7 ppm is broad). For **8**, the intensity ratios and chemical shifts of the 6, 7, and 8 + 9 carbons should be 1:1:3 at 32.0, 31.3, and 30.8 ppm, respectively, and this is the case as seen in Figure 7 and Table 2. For **9**, the ratios should be 1:1:4 for the 6, 7, and 8 + 9 carbons, respectively. However, carbons 7, 8, and 9 overlap at 30.8 ppm (broad) and so the ratio of peaks at 30.8 and 32.0 ppm appears more like 1:1+4.

Overall, the peak assignments given here are consistent with the combination of crystal packing plus conformational effects for all five model compounds. This internal consistency supports the newly determined values for the trans β sulfur shielding and γ-gauche interaction through sulfur, each of which contributes an upfield shift of ca. 0.8 ppm in the solid state. These contributions are expected to be general and of use in assignments of crystal packing and conformations in a wide variety of related thioethylene-containing materials.

Wide-Angle X-ray Scattering. The WAXS patterns of model compounds **5–9** are shown in Figure 8. The patterns are complicated, with many reflections between 4.5 and 3.7 Å, and only general trends will be discussed. The d-spacings for **5–9** calculated from the 2θ values are given in Table 3 (same order as in the figure). For all five compounds, there are five main reflections which show clear transition from **5** to **6** followed by gradual changes from **6** to **9**. The combination of peaks for **5** clearly indicates a different crystalline structure than for **6–9**, consistent with the solid-state NMR results. The peak patterns of **6–9** appear similar, with differences due mainly to overall chain length. With increase in the length of the thioethylene segment, the peaks almost all undergo a continuous shift to smaller d-values, consistent with tighter packing of all segments

Table 3. WAXD d-Spacings (Å) for Model Compounds 5–9 with the Same Order Left to Right as in Figure 8

	peak				
	1	2	3	4	5
5	4.41	4.26[a]	4.10	3.91	3.65
6	4.39	4.20?	4.20[a]	4.00	3.81
7	4.36	4.29[a]	4.20	3.92	3.70
8	4.26[a]	4.20	4.13	3.90	3.60
9	4.26	4.20[a]	4.10	3.90	3.70

[a] Most intense scattering peak.

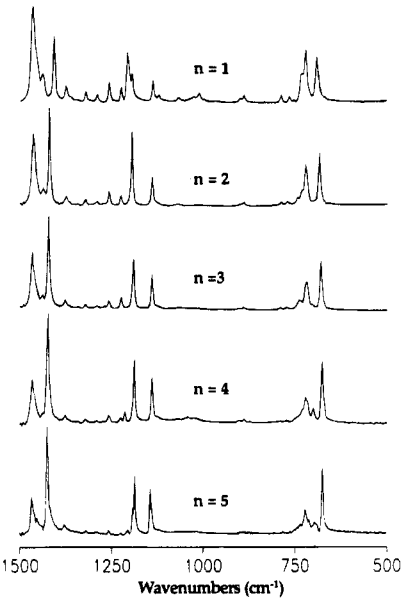

Figure 9. IR spectra of $CH_3(CH_2)_9S(CH_2CH_2S)_n(CH_2)_9CH_3$.

in the crystalline domains. This suggests increased interaction of sulfur atoms, consistent with a more rapid increase in melting points for higher oligo(thioethylene) model compounds than for the corresponding alkanes (Figure 3).

FT-IR Results. Room temperature IR spectra of **5–9** between 1500 and 500 cm^{-1} are shown in Figure 9. Overall, three key observations can be made. First, the peak at 723 cm^{-1} corresponds to the CH_2 rocking of the alkyl chains in an all-trans conformation, indicating that this is the preferred conformation for the decyl segments packed in whatever crystal forms each model compound adopts. Second, the intensity ratio of the 723 cm^{-1} band to the 1465 cm^{-1} band (CH_2 bending of the polymethylene chain) is identical for compounds **5–9**, consistent with independent behavior of the decyl chain from the thioethylene segments. Third, the increase in thioethylene units correlates with increases in bands at ca. 680, 1140, and 1420 cm^{-1} in relation to the 1465 cm^{-1} band.

The specific crystal packing difference for **5** versus the other model compounds (observed by other techniques) can also explain the significant differences in FTIR spectra. First, the peak at 1408 cm^{-1} for **5** is shifted to 1420 cm^{-1} for **6–9**. Second, the CH_2 symmetric and asymmetric wagging bands that appear as a doublet at 1208 and 1196 cm^{-1} in **5** show up as a single peak in **6–8** which gradually shifts from 1195 to 1186 cm^{-1} with increasing thioethylene segment length. In **9**, the two wagging bands are again distinct at 1191 and 1187 cm^{-1} (there are also two peaks in this region for PTE corresponding to CH_2 symmetric and asymmetric wagging). Third, the gauche content increases between compounds **6–9** are confirmed by CH_2 rocking bands

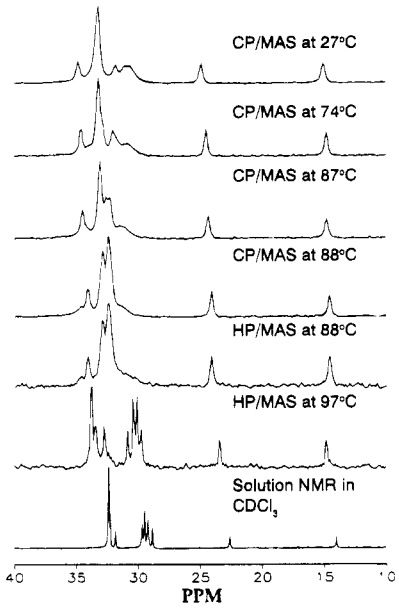

Figure 10. Variable-temperature ^{13}C CP/MAS and HPD/MAS spectra of partially deuterated $CH_3(CH_2)_9S(CH_2CH_2S)_4(CH_2)_9CH_3$ (**8′**).

at 698 cm^{-1} and a shoulder (at 716 cm^{-1}) on the peak at 723 cm^{-1} seen in **7**, **8**, and **9**. Thus, ambient temperature IR analysis supports an entirely different molecular packing for **5** and an increase in gauche thioethylene segment conformations with increase in thioethylene segment length (**6**–**9**).

Variable-Temperature Analysis of 8 and 8′. A combination of techniques was employed to monitor the individual behavior of decyl and thioethylene segments with increasing temperature. Again, it is this combination which allows elucidation of the overall molecular packing changes which occur on going through the premelt and melt transitions.

Solid-State NMR Results. Variable-temperature NMR analysis of **8′** was carried out up to the melt using ^{13}C CP/MAS and HP/MAS methods; selected spectra are given in Figure 10. The room temperature CP/MAS spectrum shows that the decyl chains are in the all-trans conformation as confirmed by the peak at 33.4 ppm.[25] The peaks corresponding to the CH_2's adjacent to the sulfur appear at 30.8 (gg), 31.3 (tg), and 31.9 ppm (tt), with the peak at 30.8 ppm being assigned to the internal C–S gauche conformers. The intensity of the peak at 30.8 ppm is reduced in **8′** as compared to **8** due to partial deuteration. On going from 27 to 74 °C (top two traces in Figure 10), there is a reduction in the intensity of the peak at 30.8 ppm (gg) and an increase in the intensity of the peak at 31.9 ppm (tt). This indicates molecular motion well below the observed DSC transition at 83–85 °C. As the energy barrier to rotation at the C–S bonds is low, gauche–trans libration is facile. This should cause a downfield shift as the γ-gauche shielding is lessened for the internal methylene units. This conformational motion at the C–S bonds leading to increase in the higher energy trans conformation also explains downfield shifting of the peak at 31.2 ppm (tg) and its merging with the peak at 31.9 ppm (tt). Thus, changes in both peak intensities and peak positions are explained by a gradual increase in the population of tt over tg and gg forms in the thioethylene segments.

Increasing the temperature to 74 °C also causes changes in the peaks of the decyl chain, which move upfield from 15.1, 25.0, 33.4, and 35.0 to 14.9, 24.6, 33.3, and 34.7 ppm, respectively. This is also due to librational motion which increases gauche-like conformations, especially at the chain ends as evidenced by appearance of a new peak (shoulder at ca. 33 ppm) that originally overlapped the main peak at 33.3 ppm. This peak corresponds to the γ-CH_2 (4) of the decyl chain, which moves upfield more due to enhanced gauche contributions at the chain ends. The methyl, α, β, and γ carbons all experience more gauche interactions than the central CH_2's as indicated by the 0.3 ppm upfield shift for the α and β carbons and the 0.1 ppm shift for the central CH_2's. This is similar to behavior in linear alkanes in which gauche imperfections increase in intensity near chain ends at high temperatures. Further increase in temperature from 74 to 87 °C (just above or at the 85 °C transition) causes the *C*–S peaks at 31.2 (gt) and 31.9 (tt) to move to 31.4 and 32.3 ppm and decreases the intensity of the peak at 31.1 ppm. The change from 31.0 ppm (at room temperature) to 32.3 ppm (at 87 °C) is due to an additive effect of γ gauche and β sulfur interactions as more and more trans isomers form at C–S bonds. The γ carbon at 87 °C has moved to 32.7 ppm, a shift of 0.6 ppm as compared to a shift of 0.1 ppm for the central carbons (third trace from the top in Figure 10). This suggests further increases in mobility and gauche conformations in the decyl chain ends. Similar changes in hexatriacontane for the γ and δ carbons have been reported, for example, with the peaks for these carbons overlapping at room temperature at ca. 33.7 ppm and moving to 32.7 and 33.3 ppm, respectively, in the *condis* (*con*formationally *dis*ordered) phase.[26]

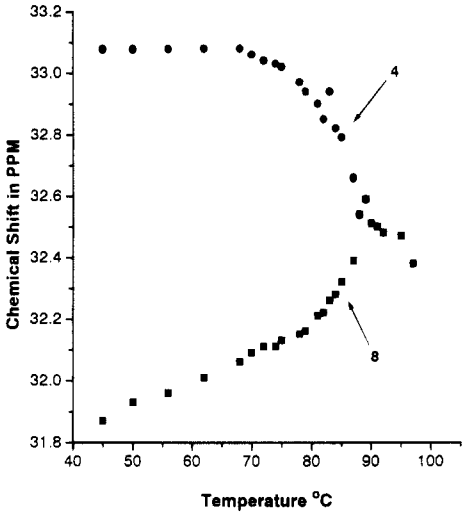

Figure 11. Temperature dependence of the chemical shifts of methylene units adjacent to sulfur in **8′**.

At 88 °C (above the premelt transition) there is complete disappearance of the peaks at 30.8 and 31.6 ppm in the CP/MAS spectrum (Figure 10, fourth trace from the top). This indicates complete conversion of gauche to trans isomers throughout the thioethylene segments. This makes all the carbons adjacent to sulfur (30.8, 31.3, and 32.0 ppm at room temperature) similar in their chemical environment so that they merge into a single, broad peak. These carbons are now similar to carbon 7 in **5** at room temperature (32.0 ppm). These downfield shifts result from loss of two γ gauche interactions and introduction of one β sulfur shielding at the internal thioethylene segments. Complete conversion to the trans form is shown in Figure 11 by the

temperature dependence of the chemical shifts of the methylene units at 30.8 ppm (at 27 °C) and 33.4 ppm (the γ CH_2, carbon 4, of the decyl chain) which moved away from the all-trans internal CH_2 peak at 33.4 ppm. Both peaks (30.8 and 33.4 ppm) exhibited gradual changes in chemical shift up to 80 °C, followed by a more rapid change up through the transition temperature. Similarly, the carbons of the terminal alkyl chain showed a continuous reduction in chemical shift up to 87 °C and then showed a discontinuous change. The peaks at 14.9, 24.4, 33.2, and 34.5 ppm jumped to 14.7, 24.2, 33.0, and 34.2 ppm on going from 87 to 88 °C. The continuous changes in chemical shift of the thioethylene segments below the premelt are due to gradual conversion of gauche to trans isomers at C–S bonds, while for the decyl chain they are due to increased librational motion causing *more* gauche interactions. The discontinuous changes in chemical shift at the transition are due to changes in long-range (intermolecular) order, which results in the high-temperature phase of **8** being similar to the room temperature structure of **5**. A structure similar to **5** should involve downfield shifts at the thioethylene segment as noticed in **8′** in going from room temperature to 88 °C. However, the chain-end carbons in **8** have increased librational motion, which causes an upfield movement from those of **5**. Thus, the chemical shifts associated with the high-temperature phase of **8** indicate a crystal structure similar to **5** at room temperature but with differences in mobility at the chain ends.

At 88 °C, only a 50% reduction in proton spin–lattice relaxation time was observed (from 8 to 4 μs). The still-efficient cross-polarization is consistent with a relatively rigid high-temperature state resulting from the solid–solid transition. When the temperature is gradually increased to 97 °C, this structure is maintained with only a ca. 0.1 ppm upfield shift for all the carbons. At 97 °C, cross-polarization is completely lost with sample melting.

^{13}C HP/MAS (high-power decoupling, no cross-polarization) spectra up to 88 °C (just above the first transition) show peaks very similar to those seen in the CP/MAS spectra (fourth and fifth traces of Figure 10). This illustrates that the observed thermal behavior is occurring homogeneously throughout the sample and is thus seen under both CP/MAS and HP/MAS conditions. Above 92 °C, the HP/MAS spectrum shows new peaks at 30.3 and 30.8 ppm due to introduction of gauche imperfections in the *central* CH_2's of the decyl chain.[26] At 97 °C, the HP/MAS spectrum looks very similar to the solution spectrum (bottom two traces in Figure 10) but shifted due to solvent effects (melt versus dissolution in $CDCl_3$). There are distinct differences between the carbons of the decyl chain and the thioethylene units on going into the melt. The thioethylene peaks move downfield while the decyl peaks move upfield. The former is due to complete elimination of both intra- and intermolecular shielding effects (similar to what occurs in solution) to give the conformationally averaged spectrum with the same relative peak positions and intensities as in the solution spectrum. Lack of solvent interactions, however, causes differences in absolute chemical shifts.

Spectra collected (both CP/MAS and HP/MAS) on cooling the sample from the melt are very similar to the spectra obtained on heating. Thus, the sample initially crystallizes into the high-temperature crystal form with all-trans conformations of both thioethylene segments and the decyl chains. At the second exotherm, the inverse of the solid–solid transition seen on heating occurs with the corresponding spectral changes. At this point, the gauche isomer population starts increasing (which allows the chains to pack closer to each other due to increased dipole interactions) as observed by increases in the peak intensity at 30.8 ppm.

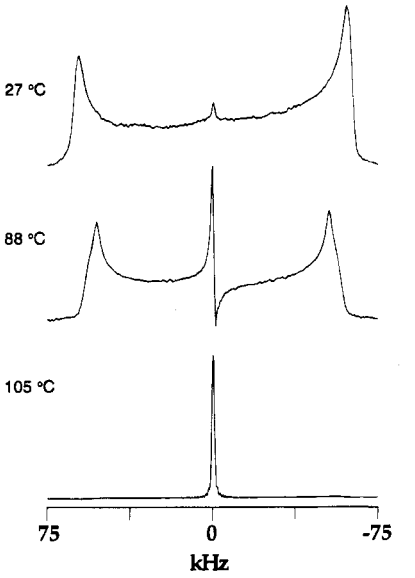

Figure 12. Variable-temperature ^2H NMR spectra of partially deuterated $CH_3(CH_2)_9S(CH_2CH_2S)_4(CH_2)_9CH_3$ (**8′**).

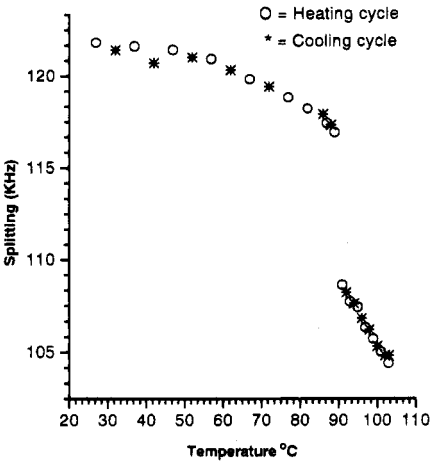

Figure 13. Temperature dependence of splitting for the C–D bond in partially deuterated $CH_3(CH_2)_9S(CH_2CH_2S)_4(CH_2)_9CH_3$ (**8′**).

To further evaluate the type and amount of molecular motion associated with the lower thermal transition, ^2H NMR analysis of **8′** was carried out. Selected spectra are given in Figure 12. At room temperature, a splitting of 118 kHz was seen, corresponding to a highly static C–D bond in a crystalline environment. As the temperature increases, a gradual, small reduction in the splitting occurred corresponding to increased librational motion up to 86 °C. ^{13}C CP/MAS and HP/MAS spectra suggest that gauche–trans isomerization or libration occurs in the solid state, but this motion is not sufficient to cause major changes in the ^2H NMR spectra up to 86 °C. At 88 °C there is a larger, discontinuous decrease in splitting to 106 kHz (Figure 13) indicating increased mobility, consistent with ^{13}C solid-state NMR data that show a 50% reduction in the proton spin–lattice relaxation time. This increased mobility is achieved through lattice expansion and reduced intermolecular interac-

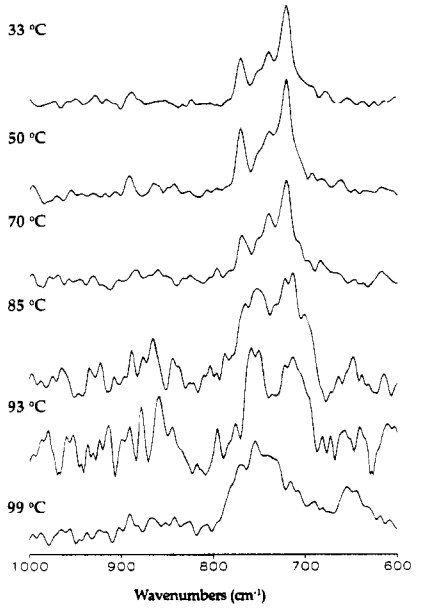

Figure 14. Raman spectra of **8′** at various temperatures.

tions. However, the splitting value (106 kHz) is several times larger than that observed for rotator[27] and liquid crystalline phases,[28] confirming that a crystalline solid–solid transition occurs at ca. 88 °C which does not involve free rotation around the chain axis. When the temperature is further increased beyond the melt (to 105 °C), a single sharp peak is observed corresponding to an isotropic motion. As the sample cools from the melt, the ^2H splitting behavior exactly parallels that seen during the heating process as can be seen in Figure 13 where the cooling cycle data overlap those of the heating cycle. This reversibility in both ^{13}C and ^2H NMR behavior shows that the phase existing *between* the two transition temperatures corresponds to a high-temperature crystal form with an all-trans conformation that is the thermodynamically stable and approachable from low or high temperatures.

Raman and FT-IR Results. High-temperature Raman analysis of **8′** was carried out up to the melt to further understand the conformational behavior at the C–S bonds (Figure 14). At 33 °C, there were four bands for the C–S bond at 771, 754, 740, and 721 cm^{-1}, corresponding to C–S asymmetric trans units, gauche (nondeuterated carbons), gauche (deuterated carbons), and C–S symmetric stretching, respectively. As the temperature increased up to 70, 80 (not shown), and 85 °C, there was reduction of the peaks at 754 and 740 cm^{-1} and growth of the 760 cm^{-1} peak, indicating increasing trans contribution at the internal C–S bonds. The C–S symmetric stretch at 713 cm^{-1} also broadened, consistent with librational motion increase. This process is even more evident above 90 °C when the C–S asymmetric peaks merged together, while in the melt (99 °C), there are two sets of multiple peaks centered at 754 and 655 cm^{-1} similar to the C–S stretches seen for liquid *n*-butyl methyl thioether.[29]

Frequency, integrated intensity, and width at half-height are the infrared parameters that are often used to study molecular motion with respect to temperature.[30] The C–H stretching mode best shows variation in intensities with respect to temperature as conformational disorder develops in the sample. A plot for **8** of integrated intensity for the C–H stretching region between 3120 and 2740 cm^{-1} versus temperature is given in Figure 15. There is continuous decrease up to

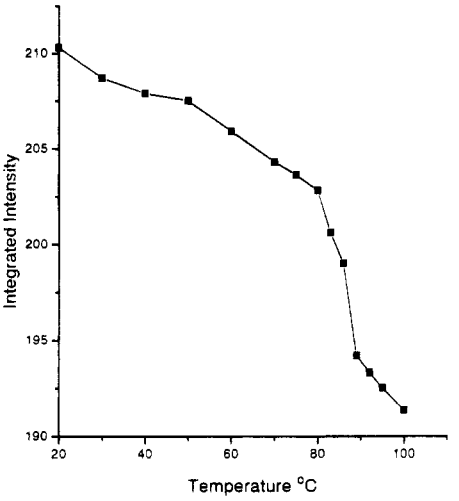

Figure 15. Integrated IR intensity versus temperature for the C–H stretching region between 3120 and 2740 cm^{-1} for **8**.

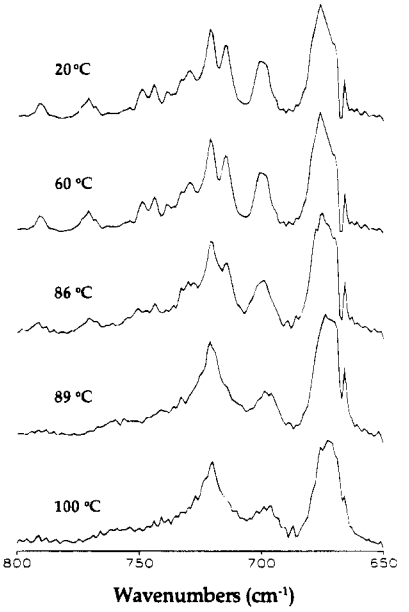

Figure 16. FT-IR spectra of **8** in the CH_2 rocking region with increasing temperature.

86 °C followed by a much faster decrease between 86 and 89 °C due to changes in packing (long-range order). The same trend is evident for the C–C stretching peaks between 1500 and 1390 cm^{-1} and C–S stretching peaks between 707 and 690 cm^{-1}. Intensity changes above the transition are very small compared to those seen in going to the rotator phases in linear alkanes, where the intensity reduction is as great as twofold.[31]

The CH_2 rocking mode is also sensitive to conformational motion in linear alkanes.[32] The CH_2 rocking modes of the gauche C–S methylenes in **8** are observed at 716 and 698 cm^{-1}, similar to those of PTE. These peaks decrease in intensity up to 86 °C (Figure 16) while at 89 °C the peak at 716 cm^{-1} is gone and that at 698 cm^{-1} is significantly reduced and shifted to lower wavenumbers. Spectra collected between the transition temperatures and down to room temperature are identical in heating and cooling cycles. A discontinuous change in integrated intensity was seen for **8′** (similar to the behavior shown for **8** in Figure 15) for the region between 800 and 600 cm^{-1}. In addition, compound **8′** displayed additional peaks between 600 and 700 cm^{-1}

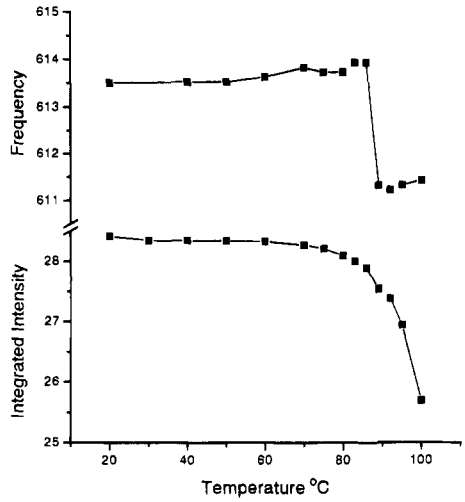

Figure 17. Temperature dependence of integrated intensity between 800 and 600 cm^{-1} (bottom trace) and frequency for the CHD rocking band (top trace) of partially deuterated $CH_3(CH_2)_9S(CH_2CH_2S)_4(CH_2)_9CH_3$ (**8′**).

for CHD rocking modes which appeared at lower wavenumbers compared to CH_2 rocking; these peaks shifted to lower wavenumber at the premelt (Figure 17). It is clear that both Raman and FT-IR analysis show increased gauche-to-trans librational motion in the thioethylene segments up to the premelt and complete conversion to a second crystal form above the transition that involves all-trans C–S bonds and decyl chain segments.

Conclusions

The lowest analog of the model compounds (**5**) has a monoclinic-like structure different from the presumed orthorhombic structures of the higher analogs as confirmed by all spectral methods used. This is due to an all-trans conformation of the thioethylene segments for this compound induced by the all-trans decyl chains on each end. Room temperature spectroscopic analysis confirms that, as the number of thioethylene segments increases, there is an increase in the number of preferred gauche conformations at the internal C–S bonds, although all thioethylenes adjacent to the decyl chains adopt a trans conformation. These conformational differences along the thioethylene segments cause differences in many key spectral parameters. ^{13}C chemical shift changes arising from γ-gauche and β sulfur interactions each give a 0.7–0.9 ppm upfield contribution. The increased amounts of gauche conformations caused by increasing numbers of thioethylene segments is also confirmed by differences in CH_2 wagging and CH_2 rocking modes in the infrared and by changes in C–S and C–H stretching vibrations in the Raman spectra. Increases in gauche conformations allow better packing and interactions between sulfur atoms, similar to that seen in poly(thioethylene) (PTE), and this results in higher melting points for the model compounds than for linear alkanes of similar lengths.

DSC analysis indicates crystal–crystal transitions for **7** and **8** at 65 and 88 °C, respectively, due to gauche to trans isomerization at the C–S bonds. This process was confirmed by variable-temperature ^{13}C CP/MAS and HP/MAS analysis of **8′**. The central carbons of the terminal decyl chains maintain their all-trans conformations through this transition, although the methyl, α, β, and γ carbons show increased mobility. At the transition, there is complete conversion to the trans form for thioethylene segments and further increase in motion at the chain ends. An expanded crystal lattice results from reduced intermolecular interactions which cause increased mobility seen by reduction in ^2H NMR peak splitting values and ^{13}C proton spin–lattice relaxation times. Variable-temperature IR and Raman results follow the same trend with complete disappearance of the vibrational modes associated with the C–S gauche units. This occurs in the solid state without greatly altering the rigidity of the lattice as seen by ^2H NMR, which showed only moderately increased librational motion up to 88 °C. The reversibility of the discontinuous, premelt process seen by DSC at 88 °C is confirmed by DSC and all of the spectroscopic techniques used.

References and Notes

(1) Mathias, L. J.; Canterberry, J. B. *Macromolecules* **1980**, *13*, 1723.
(2) Canterberry, J. B. Ph.D. Dissertation, University of Southern Mississippi, 1985.
(3) Sianawati, E.; Van De Mark, M. R. *Polym. Mater. Sci. Eng.* **1989**, *61*, 709.
(4) Sianawati, E.; Van De Mark, M. R. *J. Polym. Sci., Polym. Chem. Ed.* **1992**, *30*, 119.
(5) Angiolini, L.; Carlini, C.; Tramontini, M.; Ghedini, N. *Polymer* **1990**, *31*, 353.
(6) Yeh, J. T.; Runt, J. *J. Polym. Sci., Polym. Phys. Ed.* **1989**, *27*, 1543.
(7) Roberts, R. C. *Polymer* **1969**, *10*, 117.
(8) Mathias, L. J.; Powell, D. G.; Austran, J. P.; Porter, R. S. *Macromolecules* **1990**, *23*, 963.
(9) Cojazzi, G.; Fichera, A. M.; Malta, V.; Zanneti, R. *Makromol. Chem.* **1991**, *192*, 185.
(10) Xenopoulos, A.; Wunderlich, B. *J. Polym. Sci., Polym. Phys. Ed.* **1990**, *28*, 2271.
(11) Yagfarov, M. S. *Polym. Sci. USSR (Engl. Transl.)* **1979**, *21*, 975.
(12) Wolf, R. E.; Hartman, J. R.; Storey, J. M. E.; Foxman, B. M.; Cooper, S. R. *J. Am. Chem. Soc.* **1989**, *109*, 4328.
(13) Brown, H. C.; Rao, B. C. S. *J. Am. Chem. Soc.* **1960**, *82*, 681.
(14) Rosnati, V.; Vona, M. L.; Traldi, P. *J. Org. Chem.* **1989**, *54*, 761.
(15) Riande, E.; Guzman, J. *Macromolecules* **1981**, *14*, 1234.
(16) Riande, E.; Guzman, J. *Macromolecules* **1981**, *14*, 1511.
(17) Takahashi, Y.; Tadokoro, H.; Chatani, Y. *J. Macromol. Sci., Phys.* **1968**, *B2(2)*, 361.
(18) Nogami, N.; Sugeta, H.; Miyawaza, T. *Bull. Chem. Soc. Jpn.* **1975**, *48*, 3573.
(19) Ogawa, Y.; Ohta, M.; Sakakibara, M.; Matsuura, H.; Harada, I.; Shimanouchi, T. *Bull. Chem. Soc. Jpn.* **1977**, *50*, 650.
(20) Yokoyama, M.; Ochi, M.; Ueda, A.; Tadokoro, H. *J. Macromol. Sci., Phys.* **1973**, *B7*, 465.
(21) Grasseli, J. R.; Snavely, M. K.; Bulkin, B. J. In *Chemical Applications of Raman Spectroscopy*; Wiley-Interscience: New York, 1981; p 39.
(22) Chao, Y.; Kobayashi, M.; Tadokoro, H. *J. Chem. Phys.* **1986**, *84*, 4636.
(23) Jarrett, W. L.; Mathias, L. J.; Porter, R. S. *Macromolecules* **1990**, *23*, 5164.
(24) Jarrett, W. L.; Mathias, L. J.; Alamo, R. G.; Mandelkern, L.; Dorset, D. L. *Macromolecules* **1992**, *25*, 3468.
(25) Mathias, L. J. *Polym. Commun.* **1988**, *29*, 352.
(26) Moller, M.; Cantow, H. J.; Drottloff, H.; Emeis, D.; Lee, K.-S.; Wegner, G. *Makromol. Chem.* **1986**, *187*, 1237.
(27) Taylor, M. G.; Kelusky, E. C.; Smith, C. P. *J. Chem. Phys.* **1983**, *78*, 5108.
(28) Wann, M. H.; Harbison, G. S. *J. Am. Chem. Soc.* **1989**, *111*, 7273.
(29) Ohta, M.; Ogawa, Y.; Matsura, H.; Harada, I.; Shimanouchi, T. *Bull. Chem. Soc. Jpn.* **1977**, *50(2)*, 380.
(30) Snyder, R. G. *Macromolecules* **1990**, *23*, 2081.
(31) Casal, H. L.; Cameron, D. G.; Mantsch, H. H. *Can. J. Chem.* **1983**, *61*, 1737.
(32) Maroncelli, M.; Strauss, H. L.; Snyder, R. G. *J. Chem. Phys.* **1985**, *62*, 2812.

MA950270F